Journal of Pharmaceutical and Medical Research
Print ISSN: 2663-1954
Online ISSN: 2663-1962
DOI: https://doi.org/10.61784/jpmr3074

ALKANNIN AND ITS INHIBITORY ACTIVITY AGAINST STARCH HYDROLASES

YuJin Liu[1], WenTing Yang[1*], ZiYing Yang[1], ZiYi Zhang[1], WenJing Yao[1], Pin Guo[1], Ang Zhang[2]
[1]*School of Environmental and Biological Engineering, Wuhan Technology and Business University, Wuhan 430065, Hubei, China.*
[2]*Hubei Shenzhou Huarui Pharmaceutical Co., Ltd., Wuhan 430000, Hubei, China.*
[*]*Corresponding Author: WenTing Yang*

Abstract: This study optimized the ethanol-based ultrasonic-assisted extraction process of alkannin and evaluated its inhibitory activity and mechanism against α-amylase and α-glucosidase. The suitable ranges for various factors were determined through single-factor experiments. Subsequently, the Plackett-Burman design was employed to screen for significant factors, combined with the steepest ascent design to approach the optimal region, and the Box-Behnken design was utilized to optimize the extraction conditions. Finally, enzyme inhibition assays and molecular docking were conducted to investigate its activity and mechanism. The results indicated that the liquid-to-solid ratio, ultrasonic time, and ethanol volume fraction were significant influencing factors. The optimal extraction conditions were determined as follows: a liquid-to-solid ratio of 10:1 (mL/g), an ethanol volume fraction of 90.5%, an ultrasonic time of 45 min, and 2 extraction cycles. Under these conditions, the extraction yield of alkannin reached 1.952%. The half-maximal inhibitory concentration (IC_{50}) values of alkannin against α-amylase and α-glucosidase were 2.729 μM and 1.409 μM, respectively. Molecular docking revealed that alkannin exhibited non-competitive inhibition against α-amylase (binding energy: -6.9 kcal·mol^{-1}) and competitive inhibition against α-glucosidase (binding energy: -7.8 kcal·mol^{-1}). This study provides an experimental basis for the extraction process optimization and enzymatic inhibitory activity of alkannin.
Keywords: Alkannin; Ultrasonic-assisted extraction; Single-factor experiment; Response surface methodology; α-Amylase; α-Glucosidase; Molecular docking

1 INTRODUCTION

Alkannin is a naphthoquinone pigment extracted from the roots of *Arnebia euchroma* (Royle) Johnst. [1-2], which possesses various pharmacological activities, including anti-inflammatory and anti-tumor effects [3-5]. Traditional extraction methods, such as heating reflux and Soxhlet extraction, are time-consuming, energy-intensive, and prone to the degradation of thermolabile components [6-7]. In contrast, ultrasonic-assisted extraction (UAE) can be performed at room temperature and atmospheric pressure, significantly improving extraction efficiency [8].
α-Amylase and α-glucosidase are key enzymes in carbohydrate digestion, and their inhibitors can effectively delay glucose absorption. However, clinically commonly used drugs like acarbose exhibit gastrointestinal side effects, making natural enzyme inhibitors a research hotspot. This study aims to: (1) optimize the UAE process of alkannin using single-factor experiments and response surface methodology (RSM); (2) evaluate its inhibitory activity against two starch hydrolases; and (3) preliminarily elucidate the inhibition mechanism through molecular docking.

2 MATERIALS AND METHODS

2.1 Materials

Dried *Arnebia euchroma* was purchased from Bozhou Bozhongtang Pharmacy. The alkannin reference standard (purity >99%) was purchased from Shanghai Yuanye Bio-Technology Co., Ltd. α-Glucosidase, α-amylase, and acarbose (purity >95.0%) were purchased from Kuer Chemical Technology Co., Ltd., Beijing Aoboxing Biotechnology Co., Ltd., and PNJDULY, respectively. *p*-Nitrophenyl-β-D-glucopyranoside (pNPG) was sourced from Yishijiu Biological. Disodium hydrogen phosphate, sodium dihydrogen phosphate, sodium carbonate, potassium sodium tartrate, and 3,5-dinitrosalicylic acid were all of analytical grade (AR) and purchased from Tianjin Kaitong Chemical Reagent Co., Ltd.

2.2 Instruments and Equipment

KQ-3200E ultrasonic cleaner (Kunshan Jieliemei Ultrasonic Instruments Co., Ltd.); JY02S visible-ultraviolet spectrophotometer (Shanghai Spectrum Instruments Co., Ltd.); RE-52AA rotary evaporator (Shanghai Yarong Biochemical Instrument Plant); ReadMax 1200 full-wavelength microplate reader (Shanghai Shanpu Biotechnology Co., Ltd.).

2.3 Extraction and Determination of Alkannin

Dried *Arnebia euchroma* roots were crushed and passed through 12-mesh and 25-mesh sieves. Exactly 1.0 g of powder was taken and extracted via ultrasound under preset conditions. The extract was centrifuged at 4000 rpm for 15 min, and the absorbance of the supernatant was measured at 516 nm. The alkannin concentration was calculated using a standard curve. The extraction yield (%) = (Concentration × Total Volume × Dilution Factor) / Sample Mass × 100. The method for establishing the standard curve is detailed in Section 3.1.

2.4 Optimization of the Extraction Process

2.4.1 Single-factor experiments

To determine the appropriate range of levels for each factor, the impact of individual factors on the alkannin extraction yield was investigated while keeping other conditions constant. The evaluated levels were as follows: liquid-to-solid ratio (5:1, 10:1, 15:1, 20:1, 25:1 mL/g); ultrasonic time (10, 20, 30, 40, 50 min); ethanol volume fraction (80%, 85%, 90%, 95%, 100%); and number of extraction cycles (1, 2, 3, 4, 5 times).

2.4.2 Plackett-Burman Design (PBD)

The Plackett-Burman design has been widely employed for screening significant factors in extraction processes. Previous studies have compared various extraction methods for total naphthoquinones from *Arnebia euchroma* [7]. Based on the ranges determined by single-factor experiments, four factors—liquid-to-solid ratio (A, 5-15 mL/g), ultrasonic time (B, 30-50 min), ethanol volume fraction (C, 90%-100%), and extraction cycles (D, 1-3 times)—were selected for an N=12 PBD to screen for significant factors, using the alkannin extraction yield as the response value (Table 1).

Table 1 Levels and Factors of the Plackett-Burman Design

Level	A: Liquid-to-solid ratio (mL/g)	B: Ultrasonic time (min)	C: Ethanol volume fraction (%)	D: Extraction cycles
Low (-1)	5	30	90	1
High (+1)	15	50	100	3

2.4.3 Steepest ascent design

Based on the regression equation from the PBD, the partial regression coefficients and effect directions of each factor were determined. Using the most significant factor as a baseline, the step size was designed to approach the optimal response region, thereby determining the center point for the Box-Behnken design.

2.4.4 Box-Behnken Design (BBD)

According to the center point identified by the steepest ascent design, three factors—liquid-to-solid ratio (5-15 mL/g), ethanol volume fraction (90-91%), and ultrasonic time (40-50 min)—were selected for a 3-factor, 3-level BBD, consisting of 17 experimental runs (including 5 center points).

2.5 Enzyme Inhibitory Activity Assay

2.5.1 α-Amylase inhibition assay

The 3,5-dinitrosalicylic acid (DNS) method was employed. The reaction system contained 25 μL of sample (alkannin at 0.65-10.38 mg/mL or acarbose at 0.5-2.5 mg/mL), 25 μL of α-amylase (0.59 U/mL), and 50 μL of phosphate buffer (pH 6.9). After incubation at 37°C for 10 min, 100 μL of 1% starch solution was added, followed by another 10-min incubation. The reaction was terminated by adding 500 μL of DNS reagent and boiling in a water bath for 10 min, after which the absorbance was measured at 540 nm. Control groups were set for each sample concentration to eliminate color interference. The inhibition rate was calculated using Equation (1), and the IC_{50} was fitted using GraphPad Prism 8 software.

Inhibition rate (%) = $[1 - (A_1 - A_2) / (A_3 - A_4)] \times 100$ (1)

Where A_1 is the absorbance of the medicated group; A_2 is the absorbance of the medicated control group; A_3 is the absorbance of the non-medicated group; A_4 is the absorbance of the non-medicated control group.

2.5.2 α-Glucosidase inhibition assay

The *p*NPG method was used. The reaction system contained 7 μL of sample, 10 μL of α-glucosidase (1.25 U/mL), and 133 μL of phosphate buffer (pH 6.8). After incubation at 37°C for 10 min, 20 μL of 1.25 mM pNPG was added, followed by a 20-min incubation. The reaction was terminated by adding 170 μL of Na_2CO_3 solution, and the absorbance was measured at 405 nm. The inhibition rate was calculated using Equation (2).

Inhibition rate (%) = $[1 - (A_5 - A_6) / (A_7 - A_8)] \times 100$ (2)

Where A_5 is the absorbance of the medicated group; A_6 is the absorbance of the medicated control group; A_7 is the absorbance of the non-medicated group; A_8 is the absorbance of the non-medicated control group.

2.6 Molecular Docking

Molecular docking was performed using AutoDock 4.2 software. The crystal structures of α-amylase (PDB ID: 1DHK) and α-glucosidase (PDB ID: 3WY2) were retrieved from the RCSB PDB database. The structural features of α-glucosidase II have been characterized in detail [9].The structures of alkannin (CID: 72521) and acarbose (CID: 41774) were obtained from the PubChem database. Binding energies and binding sites were subsequently analyzed.

3 RESULTS AND DISCUSSION

3.1 Standard Curve of Alkannin

Exactly 6.0 mg of levorotatory alkannin reference standard was precisely weighed, dissolved in absolute ethanol, and made up to a volume of 10 mL to obtain a 0.6 mg/mL stock solution. After diluting to 0.1 mg/mL, aliquots of 0, 0.27, 0.36, 0.45, 0.54, and 0.63 mL were transferred to EP tubes, and absolute ethanol was added to bring the total volume to 0.9 mL. After mixing, a series of standard solutions were obtained. An amount of 20 μL of each solution was added to a 96-well plate in triplicate, and the absorbance was measured at 516 nm. With the alkannin concentration (*c*, mg/mL) as the X-axis and absorbance (*A*) as the Y-axis, the standard curve (Figure 1) yielded the regression equation: $A = 11.349c - 0.0017$, with $R^2 = 0.9997$. This indicated a good linear relationship within the concentration range of 0.03-0.07 mg/mL, which is consistent with HPLC-based determination methods for naphthoquinones from *Arnebia species* [10].

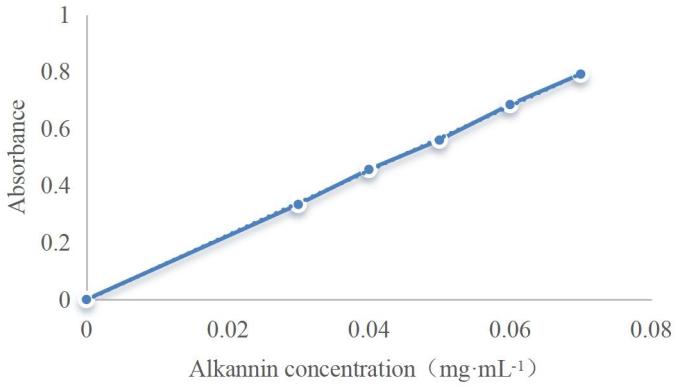

Figure 1 Standard Curve of Alkannin

3.2 Single-Factor Experiment Results

3.2.1 Effect of liquid-to-solid ratio on extraction yield

Under fixed conditions of 30 min ultrasonic time, 90% ethanol, and 3 cycles, the extraction yield initially increased and then decreased as the liquid-to-solid ratio increased from 5:1 to 25:1, peaking at 10:1 (Figure 2). A ratio too low resulted in insufficient solvent for complete dissolution, while a ratio too high decreased the ultrasonic energy per unit volume and complicated subsequent purification. Thus, 5:1, 10:1, and 15:1 were selected for subsequent studies.

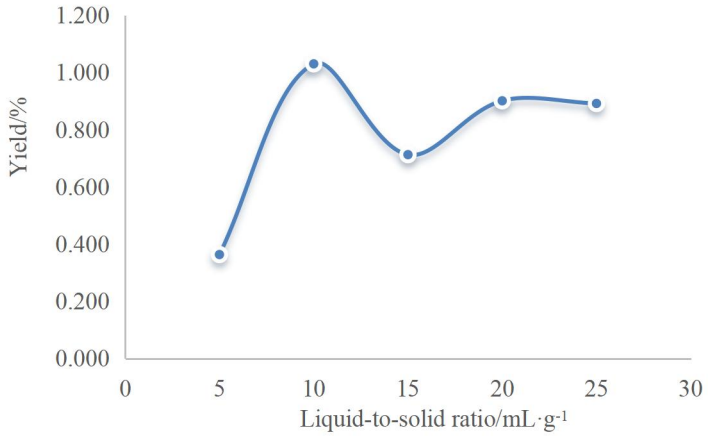

Figure 2 Effect of Liquid-To-Solid Ratio on Alkannin Extraction Yield

3.2.2 Effect of ultrasonic time on extraction yield

Under fixed conditions (ratio 10:1, 90% ethanol, 3 cycles), the yield peaked at 40 min before declining (Figure 3). Prolonged ultrasonication may destroy the chemical structure of alkannin [11]. Therefore, 30, 40, and 50 min were selected.

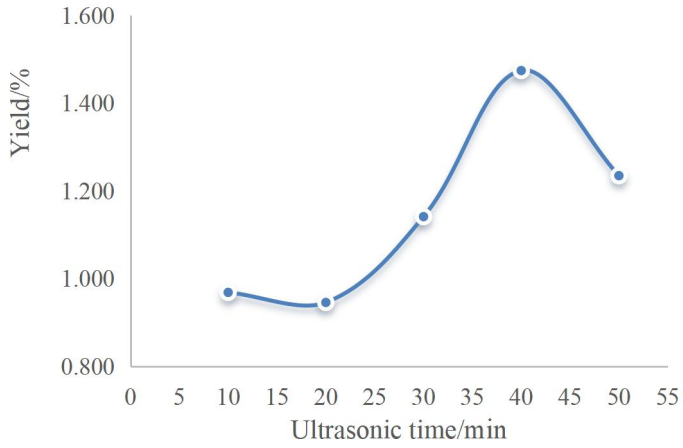

Figure 3 Effect of Ultrasonic Time on Alkannin Extraction Yield

3.2.3 Effect of ethanol volume fraction on extraction yield

Under fixed conditions (ratio 10:1, time 30 min, 3 cycles), the maximum yield was achieved at 90% ethanol (Figure 4). Higher concentrations introduced more lipophilic impurities and increased system viscosity, hindering the ultrasonic cavitation effect. The optimal ethanol concentration of 90% is comparable to that reported for alkannin extraction from two *Arnebia euchroma* varieties [12]. Thus, 90%, 95%, and 100% were selected.

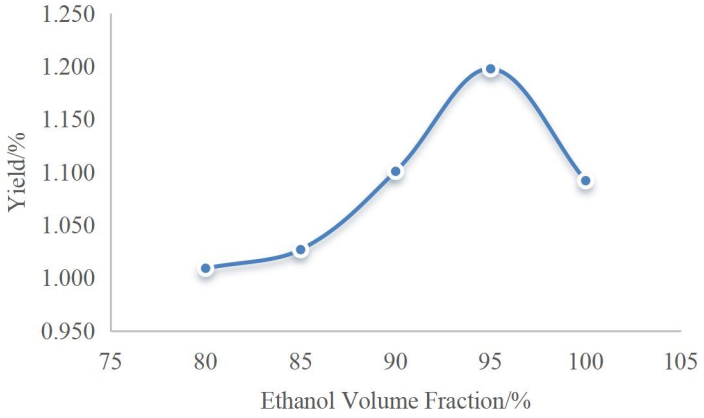

Figure 4 Effect of Ethanol Volume Fraction on Alkannin Extraction Yield

3.2.4 Effect of extraction cycles on extraction yield

Under fixed conditions (ratio 10:1, 90% ethanol, time 30 min), the yield was highest at 2 cycles (0.8625%) and subsequently decreased (Figure 5). Excessive cycling generated heat that potentially degraded alkannin. Hence, 1, 2, and 3 cycles were selected.

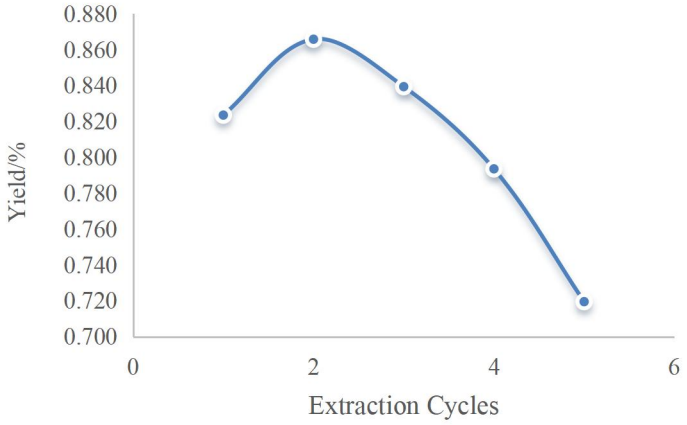

Figure 5 Effect of Extraction Cycles on Alkannin Extraction Yield

3.3 Plackett-Burman Design Results

The PBD design and results are shown in Table 2. Analysis of variance generated a half-normal probability plot (Figure 6) and a Pareto chart (Figure 7) of the standardized effects. Factors A, B, and C significantly deviated from the fitted line ($p < 0.05$), identifying the liquid-to-solid ratio, ultrasonic time, and ethanol volume fraction as critical factors. Factor D (extraction cycles) aligned with the fitted line, indicating a non-significant effect [12].

Table 2 Plackett-Burman design and results

Run	A: Ratio (mL/g)	B: Time (min)	C: Fraction (%)	D: Cycles	Extraction Yield (%)
1	1	1	1	-1	1.05
2	-1	1	1	-1	0.91
3	-1	1	1	1	1.07
4	1	-1	1	1	0.78
5	-1	-1	-1	-1	0.68
6	1	-1	-1	-1	2.21
7	-1	-1	-1	1	0.84
8	-1	1	-1	1	1.57
9	-1	-1	1	-1	0.85
10	1	1	-1	1	2.80
11	1	-1	1	1	0.76
12	1	1	-1	-1	2.11

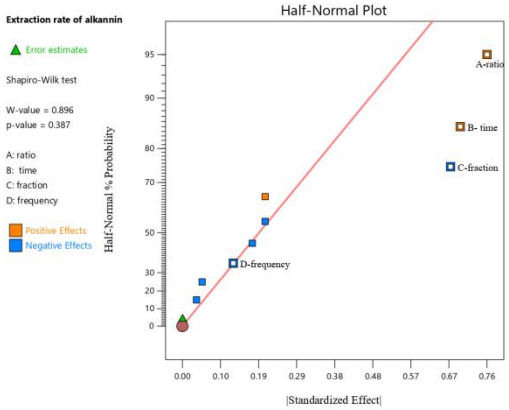

Figure 6 Half-Normal Probability Plot

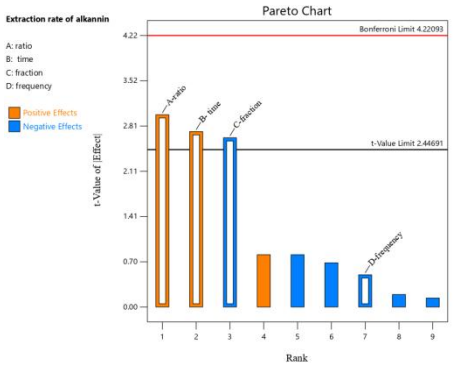

Figure 7 Pareto Chart of Standardized Effects

As shown in Table 3, the model *p*-value was 0.0236 (< 0.05). The *p*-values for A, B, and C were all < 0.05, confirming them as significant factors, whereas D was not significant ($p = 0.6351$). The regression equation was: $Y = 1.37 + 0.3802A + 0.3469B - 0.3348C - 0.0636D$. The coefficient of variation (*CV*) was 31.11%, and the adequate precision was 7.6406 (> 4), indicating a reliable model.

Table 3 ANOVA for the Plackett-Burman Design

Source	DF	Sum of Squares	Mean Square	F-value	p-value	Significance
Model	4	4.35	1.09	6.39	0.0236	Significant
A	1	1.52	1.52	8.93	0.0244	Significant
B	1	1.26	1.26	7.43	0.0343	Significant
C	1	1.18	1.18	6.92	0.0390	Significant
D	1	0.0424	0.0424	0.2496	0.6351	
Residual	6	1.02	0.17			
Lack of Fit	5	1.02	0.2039	1019.7	0.0238	Significant
Pure Error	1	0.0002	0.0002			

Total	10	5.37

3.4 Steepest Ascent Design Results

Based on the regression equation, factors A and B exhibited positive effects, while C showed a negative effect. Using factor A as the baseline (step size = 5), the step sizes for B and C were calculated. Extraction cycles were fixed at 2 (a non-significant factor at its optimal single-factor level). As shown in Table 4, Run 2 yielded the highest extraction rate (1.7424%). Therefore, the conditions of Run 2 (ratio 10:1, ethanol 90.5%, time 45 min) were selected as the center point for the BBD.

Table 4 Steepest Ascent Design and Results

Run	Step	Ratio (mL/g)	Time (min)	Fraction (%)	Yield (%)
1	0+ΔA	5	40	91.0	1.3778
2	1+ΔA	10	45	90.5	1.7424
3	2+ΔA	15	50	90.0	1.2865
4	3+ΔA	20	55	89.5	0.9893
5	4+ΔA	25	60	89.0	0.9811

3.5 Box-Behnken Design Results

The Box-Behnken design is a well-established response surface methodology for optimizing extraction conditions [14].The BBD was established with the center point determined above (Table 5). Multiple regression fitting of the data yielded the quadratic regression equation:

$Y = 1.93 - 0.0071A - 0.0384B + 0.0624C - 0.0487AB + 0.0540AC + 0.0251BC - 0.3270A^2 - 0.0581B^2 - 0.2621C^2$.

Table 5 Box-Behnken Design and Results

Run	A: Ratio (mL/g)	B: Fraction (%)	C: Time (min)	Yield (%)
1	15	90.0	45	1.6434
2	15	91.0	45	1.4372
3	10	90.5	45	1.9274
4	10	91.0	40	1.4939
5	10	90.0	40	1.5890
6	5	90.0	45	1.5726
7	5	90.5	50	1.3443
8	10	90.5	45	1.9415
9	15	90.5	50	1.4504
10	10	90.5	45	1.9468
11	10	91.0	50	1.6983
12	10	90.0	50	1.6930
13	5	91.0	45	1.5611
14	10	90.5	45	1.9380
15	5	90.5	40	1.3567
16	15	90.5	40	1.2469
17	10	90.5	45	1.9397

The ANOVA (Table 6) showed that the model was highly significant ($p < 0.0001$), while the lack of fit was not significant ($p = 0.052 > 0.05$). The R^2 was 0.9952, and the adjusted R^2 was 0.989, indicating that the model could explain 98.9% of the response value variation. The order of influence of the factors was: ultrasonic time(C) > ethanol volume fraction (B) > liquid-to-solid ratio (A).

Table 6 ANOVA for the Box-Behnken Design

Source	DF	Sum of Squares	Mean Square	F-value	p-value	Significance
Model	9	0.8816	0.098	160.5	< 0.0001	Highly Sig.
A	1	0.0004	0.0004	0.6607	0.4431	
B	1	0.0118	0.0118	19.37	0.0032	Sig.
C	1	0.0312	0.0312	51.10	0.0002	Sig.
AB	1	0.0095	0.0095	15.53	0.0056	Sig.
AC	1	0.0117	0.0117	19.09	0.0033	Sig.
BC	1	0.0025	0.0025	4.13	0.0817	
A^2	1	0.4503	0.4503	737.85	< 0.0001	Sig.
B^2	1	0.0142	0.0142	23.26	0.0019	Sig.
C^2	1	0.2892	0.2892	473.79	< 0.0001	Sig.
Residual	7	0.0043	0.0006			
Lack of Fit	3	0.0041	0.0014	26.78	0.052	Not Sig.

Based on the regression equation, response surface plots were generated to visually illustrate the effects of factor interactions on the alkannin extraction yield. Figure 8 illustrates the interactive effect of liquid-to-solid ratio and ethanol volume fraction on the extraction yield. With ultrasonic time fixed at the center level (45 min), the extraction yield remained low when the liquid-to-solid ratio was either low (5:1-8:1) or high (12:1-15:1), regardless of the ethanol volume fraction. A distinct convex region appeared when the liquid-to-solid ratio was in the mid-range (8:1-12:1) and the ethanol volume fraction approached 90.5%, where the extraction yield reached its maximum. The elliptical contour lines indicated a significant interaction between the liquid-to-solid ratio and ethanol volume fraction (p = 0.0056), which was consistent with the significance of the AB interaction term in the ANOVA.

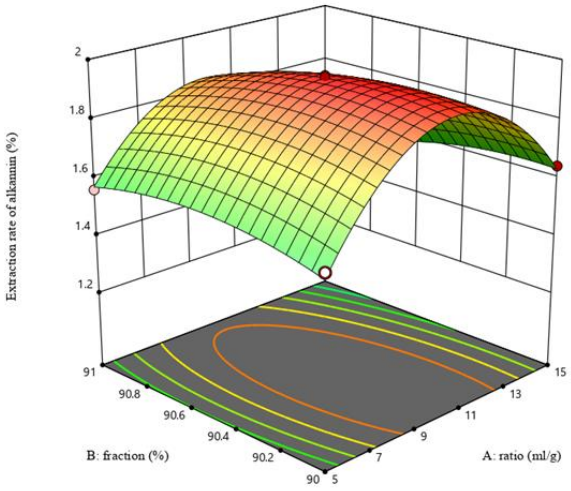

Figure 8 Response Surface Plot Showing the Effect of Liquid-To-Solid Ratio and Ethanol Volume Fraction on Alkannin Extraction Yield

Figure 9 demonstrates the interactive effect of liquid-to-solid ratio and ultrasonic time on the extraction yield. With ethanol volume fraction fixed at the center level (90.5%), the extraction yield initially increased and then decreased as both factors increased. A distinct peak region, where the extraction yield exceeded 1.94%, was observed when the liquid-to-solid ratio ranged from 8:1 to 12:1 and the ultrasonic time ranged from 42 to 48 min. The elliptical contour lines suggested a significant interaction between the liquid-to-solid ratio and ultrasonic time (p= 0.0033). Notably, ultrasonic time had a more pronounced effect on the extraction yield than liquid-to-solid ratio, as indicated by the steeper slope of the response surface along the ultrasonic time axis.

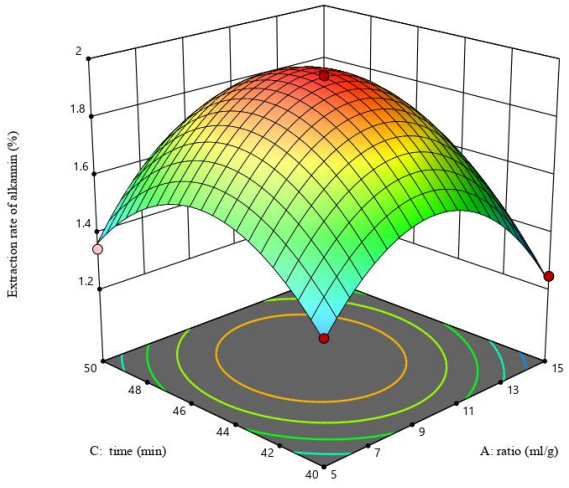

Figure 9 Response Surface Plot Showing the Effect of Liquid-To-Solid Ratio and Ultrasonic Time on Alkannin Extraction Yield

Figure 10 presents the interactive effect of ethanol volume fraction and ultrasonic time on the extraction yield. With the liquid-to-solid ratio fixed at the center level (10:1), the extraction yield was highly sensitive to changes in both factors. The maximum extraction yield was achieved when the ethanol volume fraction was between 90.3% and 90.7% and the ultrasonic time was between 43 and 47 min. Deviations from this region resulted in a marked decrease in the yield. Although the contour lines were elliptical, the p-value for the BC interaction term was 0.0817 (> 0.05), indicating that the interaction between ethanol volume fraction and ultrasonic time was not significant. Nevertheless, the shape of the

surface revealed that ultrasonic time had a greater influence on the extraction yield than ethanol volume fraction, which was consistent with the ANOVA results showing a larger F-value for C (51.10) than for B (19.37).

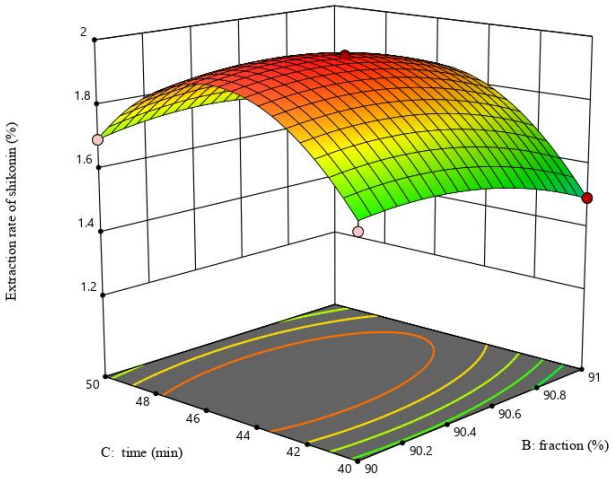

Figure 10 Response Surface Plot Showing the Effect of Ethanol Volume Fraction and Ultrasonic Time on Alkannin Extraction Yield

Taken together, the response surface analysis in Figures 8–10 clearly identified the region of maximum extraction yield within the experimental range: liquid-to-solid ratio of 9:1–11:1, ethanol volume fraction of 90.3%–90.7%, and ultrasonic time of 43–47 min. This region was in excellent agreement with the model-predicted optimal conditions (liquid-to-solid ratio of 10:1, ethanol volume fraction of 90.5%, and ultrasonic time of 45 min).

3.6 Determination and Verification of Optimal Conditions

The model predicted the optimal extraction conditions as a liquid-to-solid ratio of 10:1, an ethanol volume fraction of 90.5%, an ultrasonic time of 45 min, and 2 extraction cycles, with a predicted yield of 1.947%. Three verification experiments under these conditions yielded extraction rates of 1.956%, 1.952%, and 1.948%, averaging 1.952%. The minimal relative error between the actual and predicted values confirmed the reliability of the model.

3.7 Enzyme Inhibitory Activity

3.7.1 Inhibitory effect of alkannin on α-Amylase

As shown in Table 7, both acarbose and alkannin significantly inhibited α-amylase in a dose-dependent manner. Calculated via GraphPad Prism 8, the IC_{50} of acarbose was 0.633 μM, while that of alkannin was 2.729 μM (Table 8). Although the IC_{50} of alkannin was higher than that of acarbose, they were within the same order of magnitude. The inhibitory activity of alkannin against α-amylase and α-glucosidase is comparable to that of other natural product extracts, such as *Spatholobus suberectus* extract [15].

Table 7 Inhibition Rates of Two Agents against α-Amylase

Alkannin Conc. (μM)	2.250	4.501	9.001	18.00	36.01
Inhibition (%)	38.20	41.05	49.88	53.94	64.67
Acarbose Conc. (μM)	0.925	1.851	2.775	3.700	4.625
Inhibition (%)	44.08	61.67	69.80	75.66	80.60

Table 8 IC_{50} Values against α-Amylase

Agent	IC_{50} (μM)
Acarbose	0.633
Alkannin	2.729

3.7.2 Inhibitory effect of alkannin on α-Glucosidase

Similarly, both agents demonstrated significant dose-dependent inhibition of α-glucosidase (Table 9). At an alkannin concentration of 36.01 μM, the inhibition rate reached 71.00%. The IC_{50} of acarbose against α-glucosidase was 0.5988 μM, whereas the IC_{50} of alkannin was 1.409 μM (Table 10). The inhibitory activity of alkannin against α-glucosidase is comparable to that of other natural product extracts [15].

Table 9 Inhibition Rates of Two Agents Against α-Glucosidase

Alkannin Conc. (μM)	2.250	4.501	9.001	18.00	36.01

Inhibition (%)	43.66	46.16	54.95	67.78	71.00
Acarbose Conc. (μM)	0.925	1.851	2.775	3.700	4.625
Inhibition (%)	49.64	56.93	63.66	77.31	83.41

Table 10 IC_{50} Values Against α-Glucosidase

Agent	IC_{50} (μM)
Acarbose	0.5988
Alkannin	1.409

3.8 Molecular Docking Analysis

The endogenous substrates for α-amylase (1DHK) and α-glucosidase (3WY2) are NAG and BGC, respectively, both of which are hydrolyzed into glucose.

As illustrated in Figure 11 and Table 11, alkannin bound to α-amylase at a site distinct from that of the natural ligand NAG, suggesting a non-competitive inhibition mechanism. By altering the 3D conformation of α-amylase, alkannin reduced the enzyme's affinity for NAG. The binding energy of alkannin with α-amylase was -6.9 kcal·mol^{-1}, lower (more stable) than that of NAG (-5.8 kcal·mol^{-1}).

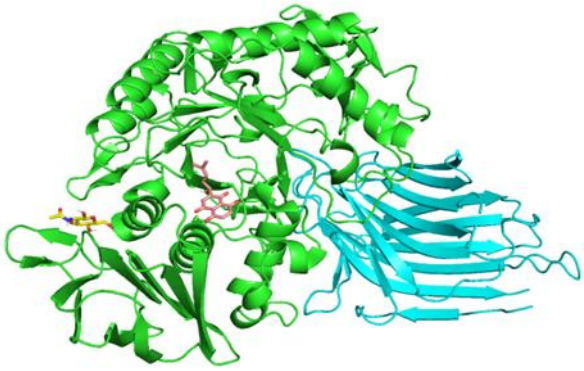

Figure 11 Molecular Docking of 1DHK-NAG-Alkannin

Conversely, alkannin bound to α-glucosidase at the same active site as BGC (Figure 12), indicating competitive inhibition. Alkannin competes with BGC to occupy the functional region of the enzyme. The binding energy of alkannin with α-glucosidase was -7.8 kcal·mol^{-1}, which was lower (more stable) than that of BGC (-6.0 kcal·mol^{-1}). Acarbose also bound to the same site as BGC (Figure 13) via competitive inhibition. HIS-348 was identified as a potentially key amino acid residue for inhibiting 3WY2 hydrolytic activity.

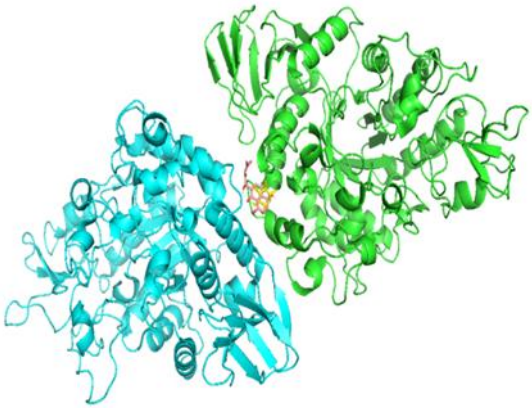

Figure 12 Molecular Docking of 3WY2-BGC-Alkannin

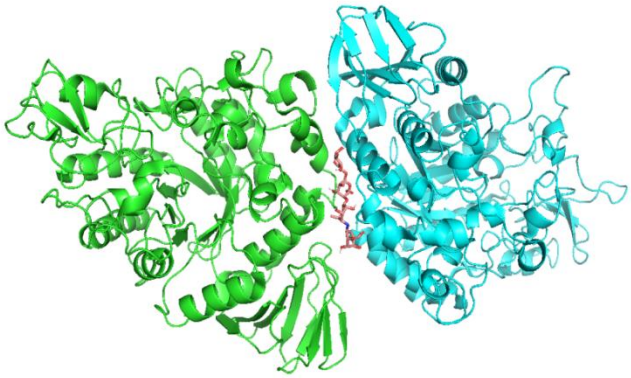

Figure 13 Molecular Docking of Acarbose and 3WY2

Notably, the binding energy of acarbose with 3WY2 (-9.5 kcal·mol⁻¹) was lower than that of alkannin (-7.8 kcal·mol⁻¹), indicating that acarbose binds more stably to the enzyme. This is consistent with the *in vitro* results where acarbose exhibited a lower IC_{50} value.

Table 11 Molecular docking results of α-glucosidase and α-amylase

Target Enzyme	Ligand	Binding Energy (kcal·mol⁻¹)	Binding Amino Acid Residues
α-Glucosidase (3WY2)	Acarbose	-9.5	ARG-437, ARG-429, HIS-348, ASN-447, ARG-450, ASP-440, GLN-349, ASN-443, ASN-46
α-Glucosidase (3WY2)	Alkannin	-7.8	HIS-348, LYS-352, ASP-441, THR-445
α-Glucosidase (3WY2)	BGC	-6.0	LYS-352, HIS-348, ARG-437, ASP-441
α-Amylase (1DHK)	Alkannin	-6.9	LYS-334, ARG-398, ASP-402, GLY-403, ARG-421
α-Amylase (1DHK)	NAG	-5.8	TRP-396, LYS-457, HIS-491, GLU-493

Detailed observations of the specific binding residues further elucidated these interactions. For α-glucosidase (3WY2), acarbose interacted with an extensive network of amino acid residues, including ARG-437, ARG-429, HIS-348, ASN-447, ARG-450, ASP-440, GLN-349, ASN-443, and ASN-46 (Figure 14). In contrast, the natural ligand BGC bound at a smaller cluster of residues, specifically LYS-352, HIS-348, ARG-437, and ASP-441 (Figure 15). Alkannin shared a partially overlapping binding pocket with BGC, notably interacting with the key residues HIS-348, LYS-352, and ASP-441, while also making contact with THR-445 (Figure 16). The shared interaction with HIS-348 between alkannin, BGC, and acarbose underscores its critical role in the active site for competitive inhibition.

Regarding α-amylase (1DHK), alkannin bound to a distinct allosteric site composed of LYS-334, ARG-398, ASP-402, GLY-403, and ARG-421 (Figure 17). This binding region is entirely separate from the catalytic pocket of the natural substrate NAG, which interacted with TRP-396, LYS-457, HIS-491, and GLU-493 (Figure 18). This spatial separation structurally validates the non-competitive inhibition mechanism determined previously, confirming that alkannin reduces enzymatic activity by inducing conformational changes rather than directly blocking the active site.

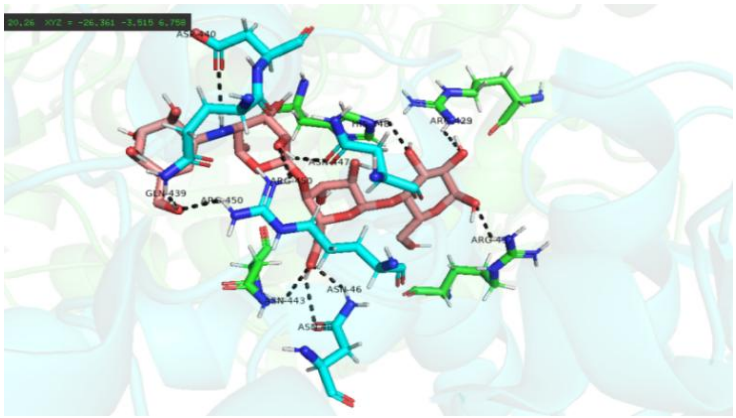

Figure 14 Amino Acid Binding Interactions between Acarbose and Target 3WY2

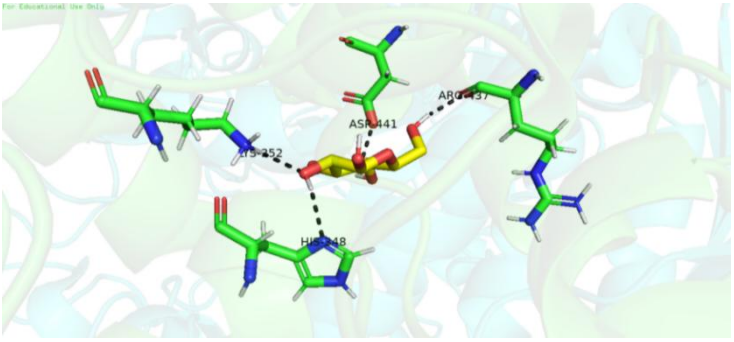

Figure 15 Amino Acid Binding Interactions between BGC and Target 3WY2

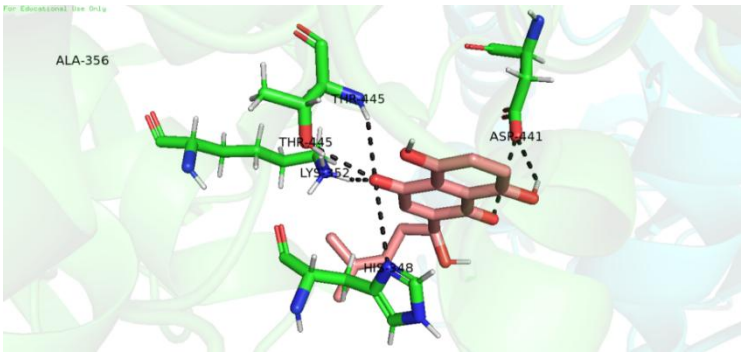

Figure 16 Amino Acid Binding Interactions between Alkannin and Target 3WY2

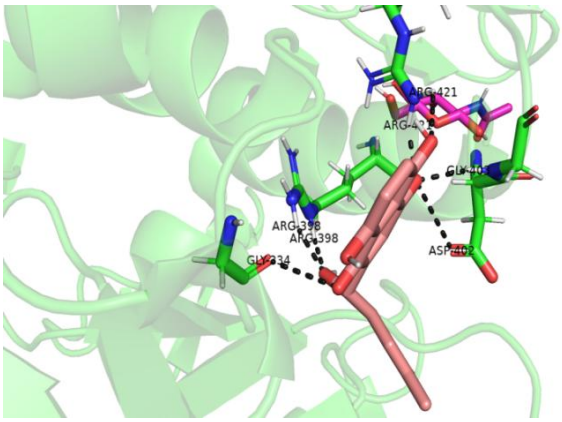

Figure 17 Amino Acid Binding Interactions between Alkannin and Target 1DHK

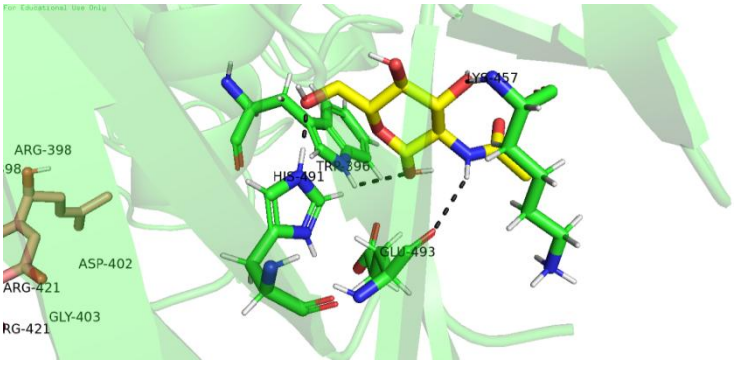

Figure 18 Amino Acid Binding Interactions between NAG and Target 1DHK

4 CONCLUSIONS AND PROSPECTS

In this study, the ethanol-based ultrasonic-assisted extraction of alkannin was optimized using Plackett-Burman, steepest ascent, and Box-Behnken designs. The optimal extraction conditions were determined as follows: an extraction time of 45 min, a liquid-to-solid ratio of 10:1, an ethanol concentration of 90.5%, and 2 extraction cycles, achieving an alkannin extraction yield of 1.947%. This process was verified to be stable and feasible.

Alkannin demonstrated *in vitro* hypoglycemic activity, with IC_{50} values of 2.729 μM against α-amylase and 1.409 μM against α-glucosidase. Molecular docking analysis preliminarily revealed that alkannin acts as a non-competitive inhibitor of α-amylase and a competitive inhibitor of α-glucosidase.

This study only preliminarily analyzed the inhibition mechanism via molecular docking. Future research should incorporate enzyme inhibition kinetics, combined with UV and fluorescence spectroscopy, to further elucidate the *in vitro* hypoglycemic mechanism. Furthermore, *in vivo* evaluations at the cellular and animal levels are warranted.

COMPETING INTERESTS

The authors have no relevant financial or non-financial interests to disclose.

FUNDING

This work was supported by the National Provincial College Students' Innovation and Entrepreneurship Training Program (202513242002) and the Scientific Research Project of the Hubei Provincial Department of Education (B2019209).

REFERENCES

[1] Lin YQ, Liu YF, Wu HZ, et al. Textual research on the nature, flavor, meridian tropism, efficacy, and medication contraindications of Lithospermum erythrorhizon. Global Traditional Chinese Medicine, 2023, 16(10): 2074-2077.
[2] Ma SJ, Geng Y, Ma L, et al. Research progress on medicinal Arnebia euchroma. Modern Chinese Medicine, 2021, 23(01): 177-184.
[3] Qian X, Li HT, Zeng WX, et al. Research progress on chemical constituents, pharmacological effects, and product applications of Lithospermum erythrorhizon. Chinese Wild Plant Resources, 2021, 40(03): 52-56+69.
[4] Wang J, Liu L, Sun XY, et al. Evidence and Potential Mechanism of Action of Lithospermum erythrorhizon and Its Active Components for Psoriasis. Frontiers in Pharmacology, 2022, 13: 781850.
[5] Kang TK, Le TT, Kwon H, et al. Lithospermum erythrorhizon Siebold & Zucc. extract reduces the severity of endotoxin-induced uveitis. Phytomedicine, 2023, 121: 155133.
[6] Ju TT, Li XD, Liu RN, et al. Research on extraction technology and application of alkannin. Feed Research, 2022, 45(17): 147-150.
[7] Yang DF. Comparison of extraction methods for total naphthoquinone from Arnebia euchroma. Journal of Shanxi Agricultural Sciences, 2019, 47(06): 1085-1086, 1091.
[8] Li LH, Fan GY, Chen H. Study on the technology of circulating ultrasonic extraction of alkannin. Journal of Zhengzhou College of Animal Husbandry Engineering, 2013, 33(01): 4-6.
[9] Ding WH, Yan XH, Ge L, et al. Determination of naphthoquinones in roots of four species of Arnebia from Xinjiang by HPLC. Chinese Traditional Patent Medicine, 2019, 41(04): 936-939.
[10] Caputo AT, Alonzi DS, Kiappes JL, et al. Structural Insights into the Broad-Spectrum Antiviral Target Endoplasmic Reticulum Alpha-Glucosidase II. Advances in Experimental Medicine and Biology, 2018, 1062: 265 -276.
[11] Wei Y, Ma HX, Shi YB, et al. Study on extraction technology of alkannin. Guangdong Chemical Industry, 2021, 48(14): 65-68, 61.
[12] Pan HL, Zhang B, Qiu LX, et al. Optimization of extraction technology and content comparison of alkannin from two kinds of Arnebia euchroma. Food Industry, 2020, 41(04): 36-39.
[13] Zhang ZW, Zhou WX, Meng JJ, et al. Optimization of extraction process of buckwheat polysaccharides by Plackett-Burman method and study on its antioxidant activity in vitro. Farm Products Processing, 2023(21): 67-73.
[14] Xu LC, Yang JY, Xu H, et al. Optimization of extraction technology of flavonoids from mango kernel by response surface methodology. China Feed, 2023(08): 18-22.
[15] Guan Y, Wang XY, Sun YY, et al. Inhibition of α-amylase and α-glucosidase by Spatholobus suberectus extract. Food and Fermentation Industries, 2023, 49(07): 126-132.